

# Communications

## Improving the Performance of Linear Inverse Solutions by Inverting the Resolution Matrix

Rolando Grave de Peralta Menendez\*, Micah M. Murray, and Sara L. Gonzalez Andino

**Abstract**—This paper proposes a new strategy for improving the localization capabilities of linear inverse solutions, based on the relationship between the real solution and the estimated solution as described by the resolution matrix equation. Specifically, we present two alternatives based on either the partial or total inversion of the resolution matrix and applied them to the minimum norm solution, which is known for its poor performance in three-dimensional (3-D) localization problems. The minimum norm transformed inverse showed a clear improvement in 3-D localization. The strong dependence of localization errors with the eccentricity of the sources, characteristic of this solution, disappears after the proposed transformation. A similar effect is illustrated, using a realistic example where multiple generators at striate areas are active. While the original minimum norm incorrectly places the generators at extrastriate cortex, the transformed minimum norm localizes, for the example considered, the sources at their correct eccentricity with very low spatial blurring.

**Index Terms**—Inverse problem, minimum norm solution, resolution matrix, source localization.

### I. INTRODUCTION

The neuroelectromagnetic inverse problem (NIP), i.e., the reconstruction of the current density vector inside the brain responsible for the electric and magnetic fields measured near/over the scalp, can be represented by a (first kind) Fredholm linear integral equation, denoting the relationship between the data measured at the external point  $d(s)$  and the superposition of the contribution of the unknown current source density distribution at locations  $r$  inside the brain [1], [2]

$$d(s) = \int_{\text{Brain}} L(s, r) \bullet j(r) dr. \quad (1)$$

The (vector) lead field function  $L(s, r)$  contains all the information about the boundary conditions, as well as the media conductivities or permittivities for the electric and magnetic cases, respectively.

Under experimental conditions, neither the measurements nor the lead field function are known for arbitrary surface/brain locations. However, assuming that the integral equation can be approximated by a discrete sum, (1) can be represented by an underdetermined system of linear equations

$$\mathbf{d} = \mathbf{L}\mathbf{j}. \quad (2)$$

Manuscript received June 20, 2003; revised February 1, 2004. This work was supported in part by the Swiss National Foundation under Grant 3152A0-100745, in part by the MHV Foundation under Grant 3234-069264.02/1, and in part by IM2 WP. Asterisk indicates corresponding author.

\*R. G. de Peralta Menendez is with the Functional Brain Mapping Laboratory, Geneva University Hospital, 1211 Geneva, Switzerland (e-mail: Rolando.Grave@hcuge.ch).

M. M. Murray was with the Functional Brain Mapping Laboratory, Geneva University Hospital, 1211 Geneva, Switzerland. He is now with the Centre Hospitalier Universitaire Vaudois, Switzerland (e-mail: Micah.Murray@hospvd.ch).

S. L. G. Andino is with the Functional Brain Mapping Laboratory, Geneva University Hospital, 1211 Geneva, Switzerland (e-mail: Sara.GonzalezAndino@hcuge.ch).

Digital Object Identifier 10.1109/TBME.2004.827538

Vectors  $\mathbf{d}$  and  $\mathbf{j}$  and matrix  $\mathbf{L}$  represent the discretization of the continuous functions, i.e.,  $\mathbf{d}_k = d(s_k)$ ,  $\mathbf{j}_m = j(r_m)$ , and  $L_{km} = w_{km}L(s_k, r_m)$  and  $w_{km}$  are the quadrature weights. All linear solutions of (2) can be obtained solving a variational problem [3]. This yields the inverse matrix  $\mathbf{G}$  that, when applied to the measured data, produces the estimated current density vector  $\hat{\mathbf{j}}$ , i.e.,

$$\hat{\mathbf{j}} = \mathbf{G}\mathbf{d}. \quad (3)$$

Substitution of the measured data, as described in (2), into (3) yields the following fundamental equation for underdetermined linear systems:

$$\hat{\mathbf{j}} = \mathbf{G}\mathbf{d} = \mathbf{G}\mathbf{L}\mathbf{j} = \mathbf{R}\mathbf{j}. \quad (4)$$

Here,  $\mathbf{R} = \mathbf{G}\mathbf{L}$  denotes the resolution matrix describing the relationship between the estimates and the original magnitudes. In simpler terms, (4) tells us that our estimates separate from the original values by a factor of  $\mathbf{R}$ . The nearer this factor is to the identity matrix, the better the estimated solution resembles the original sources.

This relationship was initially noted by the Italian mathematician, Giuseppe Peano, in his work related to one particular case of linear functionals, i.e., integral of functions. In 1967, Backus and Gilbert [4] used the same idea to evaluate solutions to geophysical problems. Since then, additional applications have appeared that can be included in this framework (e.g., beamformers, methods [5]) or that generalize this idea to the case of vector fields (WROP as in [6]).

In this paper, we reconsider this relationship for the development of strategies to improve the performance of linear inverse solutions. The idea is very simple. If there is a link between the real sources and the estimates, why not try to improve the estimates to make it closer to the real ones? Sections II–IV detail our proposal.

### II. BASIC EQUATIONS

Formally, (4) can be inverted to obtain the original magnitudes from the estimated ones. However, the rank of the resolution matrix cannot exceed the rank of the lead field matrix  $\mathbf{L}$ . For this reason, and exactly in the same way we do with (2), we have to consider approximate (or generalized) inverses for  $\mathbf{R}$ .

For the particular case we are interested in (i.e., the NIP), different alternatives exist, depending on the interpretation we assign to the blocks of the resolution matrix. Bearing in mind that the unknown vector  $\mathbf{j}$  corresponds to the discretization of a continuous vector field, each group of three components is associated with one location in the brain. Consequently, the resolution matrix inherits a particular structure that might influence the inversion strategy selected. In the following, we will present two approaches corresponding to partial and total inversion of the resolution matrix.

#### A. Partial Inversion Approaches

Consider the construction of an inverse solution aimed at the correct localization of single sources. The first approach consists of approximating the resolution matrix by the  $3 \times 3$  diagonal blocks. Assuming that the real source corresponds to one single source at location  $k$ , only the three components  $(k-1)*3+1$ ,  $(k-1)*3+2$  and  $(k-1)*3+3$  of vector  $\mathbf{j}$  would differ from zero. Thus, a partial inverse can be obtained by inverting the  $3 \times 3$  diagonal block associated with point  $k$ .

Denote by  $\mathbf{R}_{3k}$  the  $3 \times 3$  diagonal block associated to solution point  $k$  and compute  $\mathbf{M} = \mathbf{R}_{3k}^+$  where the superscript  $+$  denotes Moore–Penrose pseudoinversion. The inverse matrix is updated in the

following way:  $\mathbf{G}_k := \mathbf{M}\mathbf{G}_k$ , where  $\mathbf{G}_k$  stands for the three rows of the inverse associated to point  $k$ .

The row-by-row inversion, corresponding to solving the  $i$ th equation for the  $i$ th component of  $\mathbf{j}$ , can be readily calculated. The resulting matrix equation to compute this update of the inverse is  $\mathbf{G} := \mathbf{D}[\mathbf{I} - \mathbf{O}]\mathbf{G}$ , where  $\mathbf{D}$  is a diagonal matrix composed by the inverse of the elements at the main diagonal of  $\mathbf{R}$  and  $\mathbf{O}$  is a matrix with zeros in the main diagonal and the off-diagonal elements as the resolution matrix.

However, there are many arguments against the use of partial inversion by rows or by blocks. The main drawback is that they are associated with the retrieval of single sources, which we know already does not determine the behavior of a linear inverse for arbitrary source configurations [7], [8]. In practice, no partial inversion procedure seems to work for all source configurations, and for this reason we prefer the strategy described in Section II-B.

### B. Total Inversion of the Resolution Matrix

As is usual in numerical mathematics, an approximate inverse matrix can be obtained by regularizing it, i.e., making the matrix invertible by adding a relatively small perturbation. The further away the matrix is from the space of the regular matrices, the bigger the perturbation needed to regularize it. Another aspect to consider is the size of the matrix that could obstruct the inversion procedure. A solution that seems to satisfy both previous aspects is to add a diagonal perturbation matrix to the resolution matrix, i.e., invert  $(\mathbf{D} + \mathbf{R})$  where  $\mathbf{D}$  is a perturbation diagonal matrix using the following identity:

$$\begin{aligned} \mathbf{M} &= (\mathbf{D} + \mathbf{R})^{-1} = (\mathbf{D} + \mathbf{G}\mathbf{L})^{-1} \\ &= \mathbf{D}^{-1} - \mathbf{D}^{-1}\mathbf{G}[\mathbf{I} + \mathbf{L}\mathbf{D}^{-1}\mathbf{G}]^{-1}\mathbf{L}\mathbf{D}^{-1}. \end{aligned} \quad (5)$$

This equation considers only the inversion of the diagonal matrix and a matrix of size equal to the number of sensors. Using the previous formula, the update of the inverse matrix  $\mathbf{G} := \mathbf{M}\mathbf{G}$  can be performed without the explicit computation of the resolution matrix or its inverse.

## III. SIMULATION RESULTS

For reproducibility and compatibility with previous publications, we used a lead field model corresponding to the sensor configuration and solution space described in ISBET Newsletter 6, [7], and [8]. Specifically, this entailed a unit radius three-shell spherical head model [9] with solution points confined to a maximum radius of 0.8. The sensor configuration was comprised of 148 electrodes, and the solution space consisted of 817 points on a regular grid with an intergrid distance of 0.133 cm, corresponding to 2451 focal sources.

The basic figure of merit used to evaluate localization accuracy was the dipole localization error, defined as the Euclidean distance between the point where the maximum of the modulus of the vector field is observed and the actual source position. The errors were divided by the size of the grid unit (0.133) and were evaluated for  $x$  values in the set  $[0, 0.5, 1, 1.5, 2, 2.5, 3, 3.5, 4, 4.5, 5, 5.5, 6, 6.5, 7]$ .

For each value  $x_i$ , we computed the empirical density function and the empirical probability function defined as

$$\begin{aligned} \text{Density Function}(x_i) &= \left\{ \begin{array}{l} \% \text{ of sources with errors } \geq x_i \text{ and } < x_{i+1} \\ * \frac{100}{2451} \end{array} \right. \\ \text{Probability Function}(x_i) &= \left\{ \begin{array}{l} \% \text{ of sources with errors } \leq x_i \\ * \frac{100}{2451} \end{array} \right. \end{aligned}$$

To evaluate possible dependencies of the solution on the depth of the source, we used a measure defined as the average of the dipole localization error for the sources in an eccentricity range. This was the average dipole localization error for sources with eccentricities bigger than or

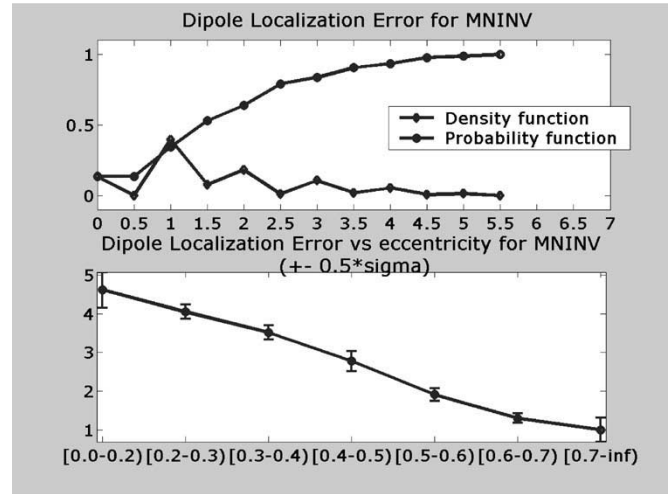


Fig. 1. Results for MNINV solution. Upper inset: Empirical distribution function and empirical probability function for the localization error. Lower inset: Average localization error as a function of the eccentricity.

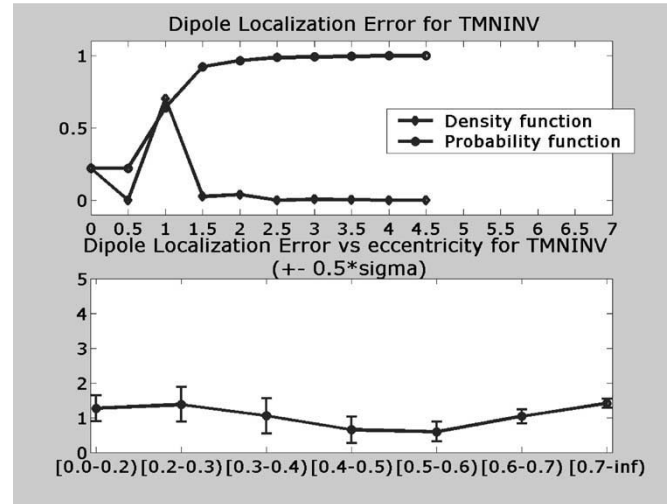


Fig. 2. Results for the TMNINV solution. Upper inset: Empirical distribution function and empirical probability function for the localization error. Lower inset: Average localization error as a function of the eccentricity.

equal to the lower limit and strictly lower than the upper limit. The eccentricity ranges considered were  $[0.0-0.2]$ ,  $[0.2-0.3]$ ,  $[0.3-0.4]$ ,  $[0.4-0.5]$ ,  $[0.6-0.7]$ , and  $[0.7-0.8]$ .

To illustrate the improvement that can be obtained with the total inversion procedure, we considered the minimum norm solution. This solution corresponds to the Moore–Penrose pseudo-inverse, that is well known for its poor performance in the localization of single sources. The perturbation matrix, i.e., the diagonal matrix that is added to regularize the resolution matrix was defined as ten times the absolute value at the main diagonal of the resolution matrix. This resulted in a diagonal-dominant matrix that was obviously invertible.

The results for the original minimum norm inverse solution (MNINV) and the transformed minimum norm inverse (TMNINV) obtained by regularizing the resolution matrix are presented in Figs. 1 and 2, respectively. Readers interested in comparing these localization results with those obtained for additional linear inverses, namely, the minimum Laplacian and the weighted minimum norm solutions, are referred to [8] and [10].

The transformed inverse (TMNINV) matrix drastically improved its localization capability of single sources with respect to the original inverse (MNINV) as revealed by the following facts.

- 1) The localization errors of the TMNINV were concentrated in the lower ranges as shown by the number of sources with zero dipole localization that increased from 13% to 22% and the sources with one unit error that increased from 34% to 70%.
- 2) The TMNINV localized more than 92% of the sources with errors lower than 1.5 grid units.
- 3) The average localization error of the TMNINV was not dependent on the eccentricity and was reduced for all eccentricity values to less than 1.4 grid units.
- 4) For the TMNINV, the higher localization errors ( $>2.5$ ) only appeared for less than 1.2% of the sources and the upper limit of maximum localization error decreased from 5.5 to 4.5.

In order to illustrate the practical consequences of using the transformed inverse (TMNINV) instead of the original minimum norm inverse (MNINV) for the localization of multiple simultaneously active sources, we have designed the simple, but nonetheless neurophysiologically plausible, example presented in Fig. 3. In this computer simulation, we calculated both inverses for a solution space of 4024 nodes homogeneously distributed within the inner compartment of a realistic head model derived from the Montreal Neurological Institute average brain (Human Brain Mapping Consortium). The solution space was restricted to the gray matter of this inner compartment and formed a regular grid of 6-mm resolution. The sensor space consisted of 111 electrodes with a spatial distribution resembling the 125-channel Geodesics Sensor Net<sup>1</sup> without its lowest electrode line.

Fig. 3(a) depicts the positions of the three simultaneously active dipoles considered. A dipole was placed within each the left and right lingual gyrus (Brodmann area 17) to mimic bilateral activation of primary visual areas (V1), and a third dipole was placed within the left superior frontal gyrus (Brodmann area 10). Note that the frontal dipole is higher along the axial direction than the visual dipoles, which is somewhat obscured by the 3-D projection used. All three dipoles had identical dipole moments in the three Cartesian components, which were set to one. In the picture, voxels represented as black circles are the ones where actual or estimated strength exceeds the 85% of the maximum strength.

Fig. 3(b) shows the localization results obtained for the original minimum norm solution, and Fig. 3(c) shows those obtained for the transformed minimum norm. Note that as predictable from its well-known limitations, the original minimum norm solution produces maxima for all the three sources at the borders of the solution space (near the sensors). This will lead to the absolutely erroneous conclusions that activity is elicited at extra striate visual areas. In contrast, the transformed solution correctly indicates bilateral activation of primary visual cortex (striate cortex), although slightly more extended than in the original source distribution, and a third source perfectly localized at the left superior frontal gyrus. Note also that the level of spatial blurring (the number of active nodes at the selected threshold) of the transformed minimum norm solution is considerably smaller than the one present in the original minimum norm reconstruction.

More importantly, this example is only illustrative and does not imply that all possible combinations of simultaneously active sources will be localized with the same accuracy.

#### IV. DISCUSSION

One important point about both the total or partial inversion of the resolution matrix deserves further discussion. Specifically, these procedures almost always transform the inverse matrix in a quasi-inverse manner, in the sense that the original system of (2) is no longer solved in the identity. Rather than being disadvantageous, this feature, common to all the Backus and Gilbert types of solutions (e.g., Beamformers and WROP), seems to be critical for the success of the inverse solution. This separation from the data results in a robust solution that might produce reliable results in the presence of noise. In fact, our experience in the

<sup>1</sup>Electrical Geodesics Incorporated, Eugene, OR.

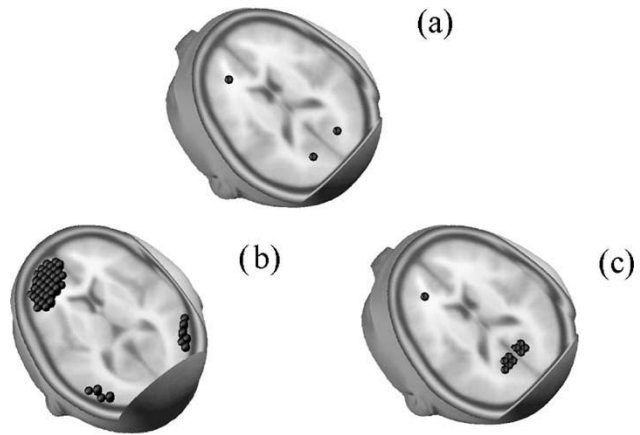


Fig. 3. Localization results for three simultaneously active sources. (a) Original three dipoles situated at the left superior frontal gyrus and left and right primary visual cortex. Note that the frontal dipole is higher along the axial direction than the visual dipoles, which is somewhat obscured by the 3-D projection used. (b) Localization results for the original minimum norm inverse (MNINV). (c) Localization results for the transformed minimum norm solution (TMNINV). Note how the original minimum norm incorrectly attribute striate cortex activation to extrastriate visual areas.

analysis of real data indicates that the updated inverse matrices obtained by inversion of (4) are more robust than inverse matrices obtained by regularization of problem (2). One could, thus, consider this new approximate inverse as a new type of regularized solution of problem (2). In fact, regularization of problem (2) is just another way to separate your inverse from the original system of equations.

This link with regularization methods suggests a clear alternative to select the perturbation matrix in the presence of noise. Representing this perturbation as the product of a diagonal matrix and an unknown factor, i.e.,  $\mathbf{D} = \alpha \mathbf{W}$ , any of the standard methods suggested to compute the regularization parameter  $\alpha$  (e.g., [11]) could be applied. The diagonal matrix  $\mathbf{W}$  can be set to the identity or to a different value according to some available *a priori* information, e.g., scaled version of the diagonal of the resolution matrix.

While the idea of inverting the resolution matrix seems to be new, this communication is by no means an exhaustive demonstration of the different inversion strategies that can be used. However, the following theoretical case is worth mentioning. When  $\mathbf{G}$  is the Moore–Penrose inverse of  $\mathbf{L}$  (as the example developed in the Section III), the Moore–Penrose inversion of  $\mathbf{R} = \mathbf{G}\mathbf{L}$  will produce the same inverse matrix and, therefore, no update. In other words, there are cases where an approximate inverse can perform better than a theoretical one.

To illustrate the method, we considered the application to the linear neuroelectromagnetic inverse problem. However, the procedures proposed here are equally valid for any inverse problem with a resolution operator associated to it.

#### ACKNOWLEDGMENT

The authors would like to thank Prof. C. M. Michel for his discussions concerning this paper.

#### REFERENCES

- [1] M. S. Hämäläinen, R. Hari, R. Ilmoniemi, R. J. Knuutila, and O. V. Lounasma, "Magnetoencephalography theory, instrumentation, and applications to non invasive studies of the working human brain," *Rev. Mod. Phys.*, vol. 65, pp. 413–497, 1993.
- [2] M. Fuchs, M. Wagner, T. Köhler, and H. A. Wischmann, "Linear and nonlinear current density reconstructions," *J. Clin. Neurophysiol.*, vol. 16, pp. 267–95, 1999.
- [3] R. G. de Peralta Menendez and S. L. G. Andino, "A critical analysis of linear inverse solutions," *IEEE Trans. Biomed. Eng.*, vol. 4, pp. 440–448, 1998.

- [4] G. E. Backus and J. F. Gilbert, "Numerical applications of a formalism for geophysical inverse problems," *Geophys. J. Roy. Astron. Soc.*, vol. 13, pp. 247–276, 1967.
- [5] K. Sekihara and B. Scholz, "Generalized wiener estimation of three dimensional current distribution from biomagnetic measurements," *IEEE Trans. Biomed. Eng.*, vol. 43, pp. 281–291, Mar. 1996.
- [6] R. G. de Peralta Menendez, O. Hauk, S. L. G. Andino, H. Vogt, and C. M. Michel, "Linear inverse solutions with optimal resolution kernels applied to the electromagnetic tomography," *Human Brain Mapping*, vol. 5, pp. 454–467, 1997.
- [7] R. G. de Peralta Menendez and S. L. G. Andino, "Discussing the capabilities of Laplacian minimization," *Brain Topogr.*, vol. 13, pp. 97–104, 2000.
- [8] R. G. de Peralta Menendez, S. L. G. Andino, G. Lantz, C. M. Michel, and T. Landis, "Noninvasive localization of electromagnetic epileptic activity. I method descriptions and simulations," *Brain Topogr.*, vol. 14, pp. 131–137, 2001.
- [9] J. P. Ary, S. A. Klein, and D. H. Fenders, "Location of sources of evoked scalp potentials: Correction for skull and scalp thicknesses," *IEEE Trans. Biomed. Eng.*, vol. BME-28, pp. 447–452, 1981.
- [10] R. G. de Peralta Menendez and S. L. G. Andino. (2002) Comparison of algorithms for the localization of focal sources: Evaluation with simulated data and analysis of experimental data. *Int. J. Bioelectromagn.* [Online]. Available: <http://www.ee.tut.fi/rgi/ijbem/volume4/number1/toc.htm>
- [11] A. R. Davies, *Optimality in Regularization. In Inverse Problems in Scattering and Imaging*, M. Bertero and E. R. Pike, Eds. New York: Adam Hilger, 1992.

## Role of Transdermal Potential Difference During Iontophoretic Drug Delivery

Andriy Bandrivskyy, Alan Bernjak, Peter V. E. McClintock, and Aneta Stefanovska\*

**Abstract**—Potential differences have been measured during transdermal iontophoresis in order to establish the effect of voltage, as opposed to current, on cutaneous blood flow. It is known that, even in the absence of drugs, the iontophoresis current can sometimes produce increased blood flow. The role of voltage in this process is studied through single-ended measurements (between electrode and body) of the potential difference during iontophoresis with 100- $\mu$ A, 20-s current pulses through deionized water, saturated 20.4% NaCl solution, 1% acetylcholine, and 1% sodium nitroprusside. It is found that the voltage needed to deliver the current varied by orders of magnitudes less than the differences in the conductance of these different electrolytes, and it is concluded that, at least for the present current protocol, the voltage as such is not an important factor in increasing the blood flow.

**Index Terms**—Blood flow, iontophoresis, laser-doppler flowmetry, transdermal potential.

Manuscript received August 20, 2003; revised February 8, 2004. This work was supported by the Engineering and Physical Sciences Research Council (U.K.), the Joy Welch Trust (U.K.), INTAS, the British Council, and the Slovenian Ministry of Education, Science and Sport. *Asterisk indicates corresponding author.*

A. Bandrivskyy and P. V. E. McClintock are with the Department of Physics, Lancaster University, Lancaster LA1 4YB, U.K.

A. Bernjak is with the Nonlinear Dynamics and Synergetics Group, Faculty of Electrical Engineering, University of Ljubljana, Tržaška 25, 1000 Ljubljana, Slovenia.

\*A. Stefanovska is with the Group of Nonlinear Dynamics and Synergetics, Faculty of Electrical Engineering, University of Ljubljana, Tržaška 25, 1000 Ljubljana, Slovenia and the Department of Physics, Lancaster University, Lancaster LA1 4YB, U.K.

TABLE I

SUMMARY OF DATA FOR THE 11 SUBJECTS, SHOWING THEIR GENDER, AGE, AND THE AVERAGE POTENTIAL DIFFERENCES (IN VOLTS) NEEDED TO DELIVER IONTOPHORESIS CURRENTS OF 100  $\mu$ A, FOR THE SIX ELECTROLYTE CONFIGURATIONS. IN EACH DATA-SET THE MEDIAN VALUE IS EMBOLDENED

Subject	gender & age	H <sub>2</sub> O (-)	H <sub>2</sub> O (+)	NaCl (-)	NaCl (+)	SNP (-)	ACh (+)
A	f, 24	<b>12.5</b>	13.8	11.1	12.1	12.2	<b>13.5</b>
B	m, 24	8.2	10.6	7.6	10.0	10.0	11.6
C	m, 24	19.9	21.3	12.8	15.5	16.6	13.8
D	m, 26	14.0	16.4	11.2	12.7	11.0	14.3
E	m, 35	11.3	<b>15.0</b>	4.2	5.9	10.7	14.3
F	f, 44	13.0	11.9	<b>9.7</b>	<b>11.1</b>	<b>9.5</b>	12.8
G	m, 45	6.7	9.7	4.8	3.1	6.5	10.7
H	m, 51	16.2	18.0	14.2	17.5	13.1	15.3
I	m, 51	8.0	15.6	10.5	7.8	7.0	7.5
J	m, 62	10.9	12.4	9.4	10.4	5.6	10.7
K	m, 68	17.1	16.8	9.5	14.6	8.5	14.1

## I. INTRODUCTION

Iontophoresis is widely used for transcutaneous delivery of ionizable drugs for the assessment of skin microvascular function. In practice, a small electrical current is used to carry e.g., vasodilators such as acetylcholine (ACh) and sodium nitroprusside (SNP) through the skin, while consequent changes in blood flow are monitored by laser Doppler flowmetry [1]–[3]. It is known, however, that increases of blood flow can be produced in response to the current, even in the absence of drugs, when using pharmacologically neutral electrolytes such as H<sub>2</sub>O [4], [5] or NaCl solution [6]. This phenomenon is known as the *galvanic effect* or *current-induced vasodilation*. The mechanism is unclear but could involve, for example, local heating due to the voltage required to convey the ions through the dermal barrier. Because a finite potential difference is always needed to maintain the chosen iontophoresis current, it is obviously important to establish whether or not the magnitude of this voltage is a significant factor in causing vasodilation.

We have therefore carried out a systematic study of the voltages needed for iontophoresis with a constant current under different conditions, and of how they change with time. The present work differs in two important respects from the investigations recently reported by Ferrell *et al.* [7] and Ramsay *et al.* [8]. First, all of our measurements are for pulsed iontophoresis, rather than for a continuous longer period of stepped current delivery. Second, our measurements are all single-ended, i.e., we measure the potential difference when a fixed current is passed between an iontophoresis cell and the body, rather than the combined voltage difference across two cells of opposite polarity, with the body in between. This enables us to establish unambiguously the voltage needed for iontophoresis of given polarity with particular electrolytes.

## II. METHODS

The measurements were performed on 11 healthy subjects (two female, nine male) aged 24–68 years (see Table I). They lay comfortably, semi-supine, with the measured forearm placed in a horizontal position on a cushion, in a quiet room with an ambient temperature of  $20 \pm 1^\circ$  C. The study was approved by the Morecambe Bay Local Research Ethics Committee and the subjects gave their fully informed consent.

Currents were derived from a battery-powered constant-current iontophoresis controller (Moor Instruments MIC1-e). The iontophoresis chambers were of perspex with internal platinum wire electrodes. Their internal diameter was 8 mm, giving an area of 1 cm<sup>2</sup> in contact with the skin. Four chambers were used, placed in a square of side 2 cm on the volar aspect of the forearm. They were held in position with double-sided adhesive disks, avoiding hair or skin defects. The earth-potential electrode was a 4 cm  $\times$  4 cm conducting pad, placed on the wrist at